Pergamon

Int. J. Solids Structures Vol. 33, No. 9, pp. 1335–1353, 1996
Elsevier Science Ltd
Printed in Great Britain

0020–7683(95)00090–9

LARGE-DEFORMATION ANALYSIS OF FLEXIBLE BEAMS

P. F. PAI
Department of Mechanical Engineering, North Carolina A&T State University, Greensboro, NC 27411, U.S.A.

and

A. N. PALAZOTTO
Department of Aeronautics and Astronautics, Air Force Institute of Technology, Dayton, OH 45433, U.S.A.

(*Received* 8 *July* 1994; *in revised form* 24 *March* 1995)

Abstract—Presented here are numerical verifications of a geometrically-exact curved beam model which fully accounts for large rotations, large displacements, initial curvatures and extensionality. A multiple shooting method is used to solve the two-point boundary-value problem of flexible beams undergoing large elastic rotations and displacements in three-dimensional space. Numerically exact large static deformations of eight beams subjected to different loading and/or boundary conditions are obtained. These solutions can be used to verify the performance of general finite-element codes in analyzing large structural deformations.

1. INTRODUCTION

Flexible structures have been used in many real-world machines. For example, leaf springs are used in the suspension systems of cars. Helical springs are used in the shock absorbers of racing motorcycles. Flexible metal strips are used in controlling the arm-type positioning mechanisms of magnetic disk drivers of computers. Transmission cables are very often subjected to large deflections. Helicopter rotor blades and wind turbine blades are flexible beams. Moreover, because of weight considerations, aircraft structures are often designed to work under postbuckling conditions. A high-altitude long-endurance (HALE) vehicle can have wing tip deflections about 25% of its wing span (Henderson, 1990).

Furthermore, the recent rapid developments in aerospace exploration have stimulated extensive research into the mechanics of large flexible space structures, such as solar collectors, dish antennas, radar arrays, truss structures, space telescopes and space stations. These space structures are usually flexible due to considerations about weight and ease of storage during launching. For example, the Radio Astronomy Explorer Satellite (Stone, 1965) used a 460 m antenna for detecting low-frequency signals. Such flexible structures can undergo large displacements and rotations without exceeding their elastic limits. To understand the behaviors of such flexible structures and to evaluate their actual load carrying capacity, more advances in modeling and computational methods are necessary.

How to deal with large rigid-body rotations is the key issue in modeling flexible structures. Since rigid-body rotations contribute no strains, strain measures to be used in modeling flexible structures need to exclude the influence of rigid-body rotations and such strains are called objective strains. Green–Lagrange strains are objective and this is the very reason why they are widely used in nonlinear structural analysis (e.g. Palazotto and Dennis, 1992). Unfortunately, Green–Lagrange strains are energy measures and hence material constants obtained in experiments by using engineering stresses and strains (they are geometric measures) cannot be directly used to relate Green–Lagrange strains to their work-conjugate stresses (i.e. second Piola–Kirchhoff stresses) in the constitutive equation. For example, Pai and Nayfeh (1994a) showed that for an isotropic prismatic bar subjected to an axial geometric strain $\varepsilon_{11} = 0.04$ (the limit of small-strain problems, according to Bathe, 1982), a 6% error is involved if a constant Young's modulus is used in the constitutive

equation of the Green–Lagrange strains and the second Piola–Kirchhoff stresses, instead of using a deformation-dependent modulus. To exclude rigid-body rotations from strain–displacement relations, Horrigmoe and Bergan (1978) and Nygard and Bergan (1989) proposed a procedure which applies a Lagrangian formulation together with a corotated "ghost" reference. Pai and Nayfeh (1991, 1994b) proposed the use of a local reference frame and local displacements in deriving objective strains and they used the derived so-called local engineering stresses and strains to derive geometrically-exact structural theories. Also, Pai and Palazotto (1995) proved that the local engineering strains are equivalent to the Jaumann strains, which are defined in continuum mechanics books (e.g. Malvern, 1969) by using the right stretch tensor from the polar decomposition of the deformation gradient tensor. Moreover, Pai and Palazotto (1995) showed that Jaumann strains (or local engineering strains) are objective geometric measures and can be easily derived by using the concept of local displacements without performing any polar decomposition. It happens that the local reference frame used by Pai and Nayfeh (1991, 1994b) is similar to the corotated "ghost" reference frame used by Nygard and Bergan (1989). However, the "ghost" reference frame is chosen such that its rotation represents the average rotation of the deformed frame, and the local reference frame used by Pai and Nayfeh (1991, 1994b) is located such that the Jaumann strain tensor is symmetric (Pai and Palazotto, 1995).

In analyzing large static deformations of flexible structures, finite-difference methods, finite-element methods and some numerical methods are usually used. For example, Minguet and Dugundji (1990) used the finite-difference method to solve fully nonlinear beam equations directly for large static deflections. The finite-element method is the mostly used method in analyzing nonlinear structures (e.g., Oden, 1972; Bathe, 1982; Bauchau and Hong, 1987; Stemple and Lee, 1988; Wriggers and Simo, 1990; Atilgan and Hodges, 1991; Palazotto and Dennis, 1992). Holden (1972) solved for large static beam deflections by using a fourth-order Runge–Kutta integration method and Wang (1991) used the fifth-order Runge–Kutta–Fehlberg method. Goto *et al.* (1992) used a combination of the transfer matrix technique (Pestel and Leckie, 1963) and the incremental arc-length method (Riks, 1979) to study the so-called limit–load instability of an elastic ring subjected to a radial twisting moment by using a nonlinear Euler–Bernoulli beam model. Although the finite-element method is still the most popular method for analyzing complex structures because of its systematic approach of treating different structural elements and system boundaries, finite-element solutions are always approximate answers because of the use of polynomial shape functions and variational formulations. Moreover, using different stress and strain measures, different methods of meshing the geometric domain, different iteration methods in solving nonlinear algebra equations and even different methods of tracing the equilibrium path can result in different solution errors in finite-element analyses. Hence, some exact solutions are useful in order to check finite-element codes.

The objectives of this paper are to provide some numerical verifications of the curved beam model of Pai and Nayfeh (1994b) by using a multiple shooting method and then to obtain large-deformation solutions to some beam problems to be used for comparison in verifying the performance of finite-element codes. Especially, we are interested in obtaining the solution of the problem studied by Goto *et al.* (1992) since nonlinear geometric coupling between bending and torsion as well as highly large displacements and rotations are involved in this particular problem.

2. GOVERNING EQUATIONS

In modeling a naturally curved and twisted beam as shown in Fig. 1, Pai and Nayfeh (1994b) used three coordinate systems. The system xyz is an orthogonal curvilinear coordinate system, where the axis x denotes the undeformed reference line of the beam and s is the undeformed arc length from the root of the beam to the reference point on the observed cross section. The system XYZ is a rectangular coordinate system used for reference purpose in calculating initial curvatures. Moreover, the system $\xi\eta\zeta$ is a local orthogonal curvilinear coordinate system, where the axis ξ represents the deformed reference line and the axes η and ζ represent the deformed configurations of the axes y and z only if there were no shear

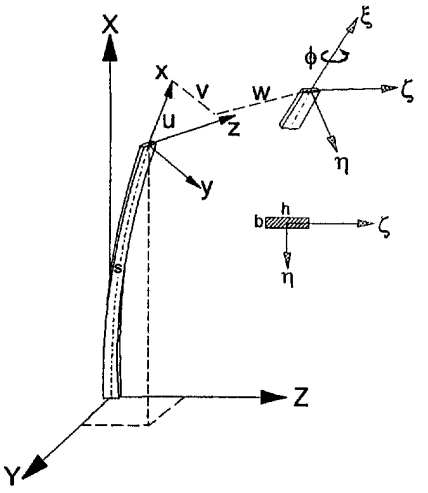

Fig. 1. Coordinate systems: XYZ is a rectangular frame; xyz is an orthogonal curvilinear frame, where the x axis represents the undeformed reference line and the y and z axes are on the observed cross-section and perpendicular to x; and $\xi\eta\zeta$ is a local orthogonal curvilinear coordinate system, where the ξ axis represents the deformed reference line.

and torsional warpings. Moreover, $\mathbf{i}_x$, $\mathbf{i}_y$ and $\mathbf{i}_z$ are unit vectors along the axes x, y and z, respectively and $\mathbf{i}_1$, $\mathbf{i}_2$ and $\mathbf{i}_3$ are unit vectors along the axes ξ, η, and ζ, respectively. It can be shown that (Reissner, 1973; Pai and Nayfeh, 1994b):

$$\frac{\mathrm{d}}{\mathrm{d}s}\begin{Bmatrix}\mathbf{i}_x\\ \mathbf{i}_y\\ \mathbf{i}_z\end{Bmatrix} = [k]\begin{Bmatrix}\mathbf{i}_x\\ \mathbf{i}_y\\ \mathbf{i}_z\end{Bmatrix}, \quad [k] \equiv \begin{bmatrix} 0 & k_3 & -k_2 \\ -k_3 & 0 & k_1 \\ k_2 & -k_1 & 0 \end{bmatrix}, \tag{1}$$

where k_1 is the initial twisting curvature and k_2 and k_3 are the initial bending curvatures. Moreover, the deformed coordinate system $\xi\eta\zeta$ and the undeformed coordinate system xyz are related by the transformation matrix $[T]$ as (Alkire, 1984; Pai and Nayfeh, 1994b)

$$\begin{Bmatrix}\mathbf{i}_1\\ \mathbf{i}_2\\ \mathbf{i}_3\end{Bmatrix} = [T]\begin{Bmatrix}\mathbf{i}_x\\ \mathbf{i}_y\\ \mathbf{i}_z\end{Bmatrix} \tag{2}$$

where

$$[T] \equiv \begin{bmatrix} T_{11} & T_{12} & T_{13} \\ T_{21} & T_{22} & T_{23} \\ T_{31} & T_{32} & T_{33} \end{bmatrix}$$

$$= \begin{bmatrix} 1 & 0 & 0 \\ 0 & \cos\phi & \sin\phi \\ 0 & -\sin\phi & \cos\phi \end{bmatrix}\begin{bmatrix} T_{11} & T_{12} & T_{13} \\ -T_{12} & T_{11}+T_{13}^2/(1+T_{11}) & -T_{12}T_{13}/(1+T_{11}) \\ -T_{13} & -T_{12}T_{13}/(1+T_{11}) & T_{11}+T_{12}^2/(1+T_{11}) \end{bmatrix} \tag{3}$$

$$T_{11} = \frac{1+u'-vk_3+wk_2}{1+e}, \quad T_{12} = \frac{v'+uk_3-wk_1}{1+e}, \quad T_{13} = \frac{w'-uk_2+vk_1}{1+e}. \tag{4}$$

Here, u, v and w are the displacements of the observed reference point with respect to the axes x, y and z, respectively, e is the axial strain on the reference line, ϕ is an Euler angle related to the twisting with respect to the deformed reference axis ξ and $(\,)' \equiv \partial(\,)/\partial s$. It follows from eqn (3) that T_{2i} and T_{3i} can be represented in terms of T_{11}, T_{12}, T_{13} and ϕ as

$$
\begin{aligned}
T_{21} &= -\cos\phi T_{12} - \sin\phi T_{13} \\
T_{22} &= \cos\phi\left(T_{11} + \frac{T_{13}^2}{1+T_{11}}\right) - \sin\phi\frac{T_{12}T_{13}}{1+T_{11}} \\
T_{23} &= \sin\phi\left(T_{11} + \frac{T_{12}^2}{1+T_{11}}\right) - \cos\phi\frac{T_{12}T_{13}}{1+T_{11}} \\
T_{31} &= \sin\phi T_{12} - \cos\phi T_{13} \\
T_{32} &= -\sin\phi\left(T_{11} + \frac{T_{13}^2}{1+T_{11}}\right) - \cos\phi\frac{T_{12}T_{13}}{1+T_{11}} \\
T_{33} &= \cos\phi\left(T_{11} + \frac{T_{12}^2}{1+T_{11}}\right) + \sin\phi\frac{T_{12}T_{13}}{1+T_{11}}.
\end{aligned} \tag{5}
$$

Because $[T]$ is a unitary matrix, we have the identity

$$
[T]^{\mathrm{T}} = [T]^{-1}. \tag{6}
$$

Differentiating eqn (2) with respect to s and using eqns (2) and (1), we obtain

$$
\frac{\partial}{\partial s}\begin{Bmatrix}\mathbf{i}_1\\ \mathbf{i}_2\\ \mathbf{i}_3\end{Bmatrix} = [K]\begin{Bmatrix}\mathbf{i}_1\\ \mathbf{i}_2\\ \mathbf{i}_3\end{Bmatrix} \tag{7a}
$$

where

$$
[K] \equiv \begin{bmatrix} 0 & \rho_3 & -\rho_2 \\ -\rho_3 & 0 & \rho_1 \\ \rho_2 & -\rho_1 & 0 \end{bmatrix} = [T]'[T]^{\mathrm{T}} + [T][k][T]^{\mathrm{T}}. \tag{7b}
$$

ρ_1 is the twisting curvature and ρ_2 and ρ_3 are the bending curvatures. We note that ρ_i are not real curvatures because the differentiation is with respect to the undeformed element length $\mathrm{d}s$ and not the deformed length $(1+e)\,\mathrm{d}s$. Multiplying eqn (7b) by $[T]$ and using eqn (6) yields

$$
\begin{bmatrix} T'_{11} & T'_{12} & T'_{13} \\ T'_{21} & T'_{22} & T'_{23} \\ T'_{31} & T'_{32} & T'_{33} \end{bmatrix} = [K][T] - [T][k]. \tag{8}
$$

Using eqns (7a), (2) and (1), one can show that

$$
\begin{aligned}
\rho_1 &= \mathbf{i}_3 \cdot \mathbf{i}'_2 \\
&= (T_{31}\mathbf{i}_x + T_{32}\mathbf{i}_y + T_{33}\mathbf{i}_z) \\
&\quad \cdot [T'_{21}\mathbf{i}_x + T'_{22}\mathbf{i}_y + T'_{23}\mathbf{i}_z + T_{21}(k_3\mathbf{i}_y - k_2\mathbf{i}_z) + T_{22}(k_1\mathbf{i}_z - k_3\mathbf{i}_x) + T_{23}(k_2\mathbf{i}_x - k_1\mathbf{i}_y)] \\
&= T_{31}T'_{21} + T_{32}T'_{22} + T_{33}T'_{23} \\
&\quad + (T_{33}T_{22} - T_{32}T_{23})k_1 + (T_{31}T_{23} - T_{33}T_{21})k_2 + (T_{32}T_{21} - T_{31}T_{22})k_3 \\
&= T_{31}T'_{21} + T_{32}T'_{22} + T_{33}T'_{23} + T_{11}k_1 + T_{12}k_2 + T_{13}k_3,
\end{aligned} \tag{9}
$$

where we used the identities $\mathbf{i}_1 \times \mathbf{i}_2 = \mathbf{i}_3$, $\mathbf{i}_2 \times \mathbf{i}_3 = \mathbf{i}_1$ and $\mathbf{i}_3 \times \mathbf{i}_1 = \mathbf{i}_2$. Substituting eqn (5) into eqn (9), one can show that

$$\phi' = \rho_1 - \frac{1}{1+T_{11}}(T_{13}T'_{12} - T_{12}T'_{13}) - T_{11}k_1 - T_{12}k_2 - T_{13}k_3. \tag{10}$$

Using the extended Hamilton principle, the local engineering stresses and strains [i.e. Jaumann stresses and strains (see Malvern, 1969; Pai and Palazotto, 1995)], and a new interpretation and manipulation of orthogonal virtual rotations, Pai and Nayfeh (1994b) derived six fully non-linear equations of motion describing one extension, two bending, one torsion and two shearing vibrations. Since we consider highly thin and flexible beams, shear deformations are neglected in this paper. Without shear deformations, these governing equations can be written as

$$\frac{\partial\{F\}}{\partial s} + [K]^{\mathrm{T}}\{F\} + [T]\begin{Bmatrix} q_1 \\ q_2 \\ q_3 \end{Bmatrix} = \begin{Bmatrix} 0 \\ 0 \\ 0 \end{Bmatrix} \tag{11}$$

$$\frac{\partial\{M\}}{\partial s} + [K]^{\mathrm{T}}\{M\} + \begin{Bmatrix} 0 \\ -(1+e)F_3 \\ (1+e)F_2 \end{Bmatrix} + \begin{Bmatrix} q_4 \\ q_5 \\ q_6 \end{Bmatrix} = \begin{Bmatrix} 0 \\ 0 \\ 0 \end{Bmatrix} \tag{12}$$

where $\{F\} \equiv \{F_1, F_2, F_3\}^T$, $\{M\} \equiv \{M_1, M_2, M_3\}^T$, F_i are the stress resultants, and M_i are the stress moments. We note that eqns (11) and (12) are the same as those derived by Reissner (1973) (when shear deformations are excluded) by using another approach. The stress resultants and moments are defined as

$$\begin{Bmatrix} F_1 \\ M_1 \\ M_2 \\ M_3 \end{Bmatrix} = \int_A \begin{Bmatrix} \sigma_{11} \\ y\sigma_{13} - z\sigma_{12} \\ z\sigma_{11} \\ -y\sigma_{11} \end{Bmatrix} \mathrm{d}y\,\mathrm{d}z \tag{13}$$

where A denotes the cross-section area and σ_{ij} are Jaumann stresses. F_2 and F_3 are transverse shear resultants, which can be represented in terms of stress moments and their derivatives by using eqn (12). It is inappropriate to represent F_2 and F_3 in terms of transverse shear stresses because transverse shear strains and hence transverse shear stresses are neglected in the Euler–Bernoulli beam theory. Furthermore, q_1, q_2 and q_3 are distributed external forces acting along the axes x, y and z, respectively, and q_4, q_5 and q_6 are distributed external moments acting along the axes ξ, η, and ζ, respectively.

For isotropic beams, the constitutive equation is

$$\begin{Bmatrix} \sigma_{11} \\ \sigma_{12} \\ \sigma_{13} \end{Bmatrix} = \begin{bmatrix} E & 0 & 0 \\ 0 & G & 0 \\ 0 & 0 & G \end{bmatrix} \begin{Bmatrix} \varepsilon_{11} \\ \varepsilon_{12} \\ \varepsilon_{13} \end{Bmatrix}, \tag{14}$$

where ε_{ij} are Jaumann strains, E is Young's modulus, G is the shear modulus and $\sigma_{22} = \sigma_{33} = \sigma_{23} = 0$ is assumed. The strain–displacement relations are (Pai and Nayfeh, 1994b)

$$\begin{aligned} \varepsilon_{11} &= e + z(\rho_2 - k_2) - y(\rho_3 - k_3) + (\rho_1 - k_1)'g \\ \varepsilon_{12} &= (\rho_1 - k_1)(-z + g_y) \\ \varepsilon_{13} &= (\rho_1 - k_1)(y + g_z), \end{aligned} \tag{15}$$

where $g(y, z)$ is a torsion-induced out-of-plane warping function, $g_y \equiv \partial g/\partial y$ and $g_z \equiv \partial g/\partial z$.

Substituting eqns (14) and (15) into eqn (13), neglecting the influence of torsional warping on ε_{11} (i.e. setting $(\rho_1 - k_1)' = 0$) and assuming that the cross section is a rectangular one having width b along the axis y and thickness h along the axis z and that the reference axis passes through the area centroid, we obtain that

$$\begin{Bmatrix} F_1 \\ M_1 \\ M_2 \\ M_3 \end{Bmatrix} = \begin{bmatrix} EA & 0 & 0 & 0 \\ 0 & G\hat{J} & 0 & 0 \\ 0 & 0 & EI_{22} & 0 \\ 0 & 0 & 0 & EI_{33} \end{bmatrix} \begin{Bmatrix} e \\ \rho_1 - k_1 \\ \rho_2 - k_2 \\ \rho_3 - k_3 \end{Bmatrix}, \tag{16}$$

where

$$I_{22} \equiv \tfrac{1}{12}bh^3, \quad I_{33} \equiv \tfrac{1}{12}hb^3,$$

$$\hat{J} = \int_A (y^2 + z^2 + yg_z - zg_y)\,\mathrm{d}y\,\mathrm{d}z = \tfrac{1}{3}bh^3\left(1 - \frac{192h}{\pi^5 b}\sum_{n=1,3,\ldots}^{\infty}\frac{1}{n^5}\tanh\frac{n\pi b}{2h}\right). \tag{17}$$

For thick curved beams, significant extension–bending couplings may exist because of the trapezoidal edge effect, which is an effect due to the fact that the undeformed element length at $(y, z) \neq (0,0)$ is not equal to that at $(y, z) = (0, 0)$. Since only thin flexible beams are considered, the trapezoidal-edge effect and hence the extension–bending coupling induced by initial bending curvatures are neglected in eqn (16). Extension–bending and extension–twist couplings induced by initial bending and twist curvatures can be important for thick and/or anisotropic beams. For these coupling effects, readers are referred to the work of Berdichevskii and Staroselsky (1979) and Cesnik and Hodges (1993). The polar moment of inertia $\hat{J}(\neq I_{22} + I_{33})$ in eqn (17) accounts for the influence of the torsional warping effect on the torsional stiffness (Timoshenko and Goodier, 1970).

Expanding eqns (11) and (12) yields

$$F_1' = \rho_3 F_2 - \rho_2 F_3 - T_{11}q_1 - T_{12}q_2 - T_{13}q_3 \tag{18a}$$

$$F_2' = \rho_1 F_3 - \rho_3 F_1 - T_{21}q_1 - T_{22}q_2 - T_{23}q_3 \tag{18b}$$

$$F_3' = \rho_2 F_1 - \rho_1 F_2 - T_{31}q_1 - T_{32}q_2 - T_{33}q_3 \tag{18c}$$

$$M_1' = \rho_3 M_2 - \rho_2 M_3 - q_4 \tag{18d}$$

$$M_2' = \rho_1 M_3 - \rho_3 M_1 + (1+e)F_3 - q_5 \tag{18e}$$

$$M_3' = \rho_2 M_1 - \rho_1 M_2 - (1+e)F_2 - q_6. \tag{18f}$$

It follows from eqn (8) that

$$T_{11}' = \rho_3 T_{21} - \rho_2 T_{31} + T_{12}k_3 - T_{13}k_2 \tag{18g}$$

$$T_{12}' = \rho_3 T_{22} - \rho_2 T_{32} + T_{13}k_1 - T_{11}k_3 \tag{18h}$$

$$T_{13}' = \rho_3 T_{23} - \rho_2 T_{33} + T_{11}k_2 - T_{12}k_1. \tag{18i}$$

Substituting eqns (18h) and (18i) into eqn (10) yields

$$\phi' = \rho_1 - T_{11}k_1 - T_{12}k_2 - T_{13}k_3 - \frac{T_{13}}{1+T_{11}}(\rho_3 T_{22} - \rho_2 T_{32} + T_{13}k_1 - T_{11}k_3) + \frac{T_{12}}{1+T_{11}}(\rho_3 T_{23} - \rho_2 T_{33} + T_{11}k_2 - T_{12}k_1). \tag{18j}$$

Moreover, it follows from eqn (4) that

$$u' = -1+vk_3-wk_2+(1+e)T_{11} \tag{18k}$$

$$v' = wk_1-uk_3+(1+e)T_{12} \tag{18l}$$

$$w' = uk_2-vk_1+(1+e)T_{13}. \tag{18m}$$

Equations (18a–m) are the 13 govern differential equations, where T_{2i} and T_{3i} are functions of T_{11}, T_{12}, T_{13} and ϕ (see eqn (5)) and it follows from eqn (16) that

$$\begin{Bmatrix} e \\ \rho_1 \\ \rho_2 \\ \rho_3 \end{Bmatrix} = \begin{bmatrix} 1/EA & 0 & 0 & 0 \\ 0 & 1/G\hat{J} & 0 & 0 \\ 0 & 0 & 1/EI_{22} & 0 \\ 0 & 0 & 0 & 1/EI_{33} \end{bmatrix} \begin{Bmatrix} F_1 \\ M_1 \\ M_2 \\ M_3 \end{Bmatrix} + \begin{Bmatrix} 0 \\ k_1 \\ k_2 \\ k_3 \end{Bmatrix}. \tag{19}$$

Hence, there are only 13 unknown dependent variables:

$$F_1, F_2, F_3, M_1, M_2, M_3, T_{11}, T_{12}, T_{13}, \phi, u, v, w.$$

The boundary conditions are of the form (Pai and Nayfeh, 1994b)

$$\begin{aligned} u = 0 \quad &\text{or} \quad F_x = \text{const.} \\ \delta v = 0 \quad &\text{or} \quad F_y = \text{const.} \\ \delta w = 0 \quad &\text{or} \quad F_z = \text{const.} \\ \delta\theta_1 = 0 \quad &\text{or} \quad M_1 = \text{const.} \\ \delta\theta_2 = 0 \quad &\text{or} \quad M_2 = \text{const.} \\ \delta\theta_3 = 0 \quad &\text{or} \quad M_3 = \text{const.} \end{aligned} \tag{20}$$

where F_x, F_y and F_z are the projections of stress resultants along the axes x, y and z, respectively, and $\delta\theta_1$, $\delta\theta_2$ and $\delta\theta_3$ are virtual rotations with respect to the axes ξ, η, and ζ, respectively. They are given by

$$\begin{aligned} F_x &\equiv F_1T_{11}+F_2T_{21}+F_3T_{31} \\ F_y &\equiv F_1T_{12}+F_2T_{22}+F_3T_{32} \\ F_z &\equiv F_1T_{13}+F_2T_{23}+F_3T_{33} \end{aligned} \tag{21}$$

$$\begin{aligned} \delta\theta_1 &= T_{31}\delta T_{21}+T_{32}\delta T_{22}+T_{33}\delta T_{23} \\ \delta\theta_2 &= -(T_{31}\delta T_{11}+T_{32}\delta T_{12}+T_{33}\delta T_{13}) \\ \delta\theta_3 &= T_{21}\delta T_{11}+T_{22}\delta T_{12}+T_{23}\delta T_{13}. \end{aligned} \tag{22}$$

It can be seen from eqn (20) that there are only 12 boundary conditions (six at each end) and hence the order of the system is 12. Consequently, only 12 of the 13 unknown variables are independent and one of the differential equations (18a–m) is redundant, which is because $\mathbf{i}_1$ is a unit vector and hence

$$T_{11}^2+T_{12}^2+T_{13}^3 = 1. \tag{23}$$

In other words, T_{11} is known when T_{12} and T_{13} are specified. However, using the 13 equations shown in eqns (18a–m) instead of using 12 equations makes the programming easier and the numerical results from the redundant equation can be used to double-check the results. But, in order to satisfy eqn (23), we use

$$T'_{11} = -\frac{T_{12}T'_{12}}{T_{11}} - \frac{T_{13}T'_{13}}{T_{11}} \tag{24}$$

in calculating T'_{11} and use eqn (18g) in calculating the Jacobian of this differential equation.

3. NUMERICAL RESULTS AND DISCUSSIONS

Since problems involving very large displacements and rotations are considered in this paper, a simple shooting method is not able to handle serious ill-conditioning problems due to nonlinearities. To solve such highly nonlinear two-point boundary value problems, we adopt the multiple shooting method and use the IMSL subroutine DBVPMS (Sewell, 1982). The problem is also parameterized by using a parameter p such that the problem is linear when $p = 0$ and the original nonlinear problem is recovered when $p = 1$. Differential equation error tolerance DTOL and boundary condition error tolerance BTOL (Sewell, 1982) are typically chosen as DTOL $= 1.0 \times 10^{-7}$ and BTOL $= 1.0 \times 10^{-5}$ for all the cases. Although there is no difficulty in obtaining any desired accuracy by using smaller values for DTOL and BTOL, using smaller DTOL and BTOL causes more computational effort with no significant change in the solution. Since the original differential equations are directly solved and any solution accuracy can be obtained, the obtained solutions are numerically exact. All the numerical results in this paper were obtained by using a 33 MHz 486 computer.

Eight cases of large static deformations are considered in this paper.

I. *Cantilever subjected to end moment* (*Fig.* 2)

In this standard example an initially straight cantilever having length L is bent into a circular arc by an bending moment at the free end. At the fixed end, because $\mathbf{i}_3 = \mathbf{i}_z$ and hence $T_{31} = T_{32} = 0$ and $T_{33} = 1$, it follows from eqn (22) that $\delta\theta_1 = \delta T_{23}$. Moreover, because $\mathbf{i}_1 = \mathbf{i}_x$ and hence $T_{11} = T_{12} = 0$ and $T_{11} = 1$, it follows from eqn (5) that $T_{23} = \sin\phi$. Consequently, the boundary condition $\delta\theta_1 = 0$ is equivalent to $\phi = 0$. Similarly, one can show that $\delta\theta_2 = -\delta T_{13}$ and $\delta\theta_3 = \delta T_{12}$. Hence, the boundary conditions are

$$\begin{aligned} &\text{at } s = 0: \quad u = v = w = \phi = T_{13} = T_{12} = 0, \quad T_{11} = 1 \\ &\text{at } s = L: \quad F_x = F_y = F_z = M_1 = M_3 = 0, \quad M_2 = n\frac{2\pi EI_{22}}{L}, \end{aligned} \tag{25}$$

where n represents a non-dimensionalized bending moment. The chosen material properties and beam geometry for Cases I–VI are

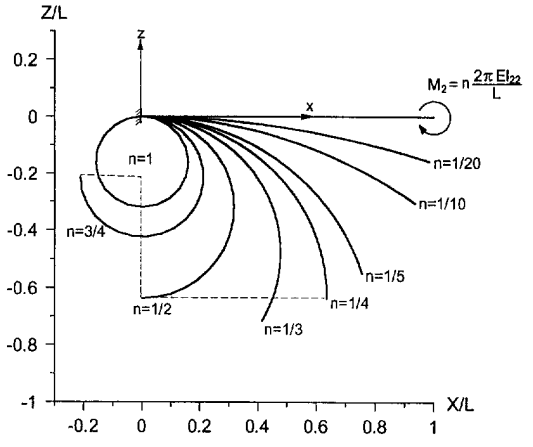

Fig. 2. The deformation of a cantilever subjected to an end moment M_2.

$$E = 1 \times 10^7 \text{ psi}, \quad \nu = 0.3 \tag{26}$$
$$b = 0.1 \text{ in}, \quad h = 0.01 \text{ in}, \quad L = 10 \text{ in}$$

where ν is Poisson's ratio. Since we use normalized variables and shear effects are neglected in this paper, the beam geometry does not influence the numerical results shown in Figs 2–9.

For this problem, the exact solution can be obtained from the governing equations (11), (12) and (16). Because of the special loading condition, $M_2(s) = M_2 = \text{constant}$ and $F_1 = F_2 = F_3 = M_1 = M_3 = 0$. Hence, it follows from eqn (16) that $e = 0$ and hence $\rho_2 = \Psi/L$, where Ψ denotes the sector angle formed by the deformed beam reference line. Consequently, it follows from eqn (16) that

$$\Psi = \frac{M_2 L}{EI_{22}}. \tag{27}$$

Figure 2 shows that the obtained numerical solutions are exactly the same as that predicted by eqn (27). However, because only 21 points (i.e. 21 shooting points) are used to describe the deformed reference axis and they are connected by straight lines, the deformed beam looks like a piecewise straight curve when M_2 is large.

II. *First-mode buckling of cantilever* (*Fig.* 3)

We consider the same cantilever shown in eqn (26) subjected to an axial load. Timoshenko and Gere (1961) used the linear Euler–Bernoulli beam theory to show that the critical buckling load F_{cr} is

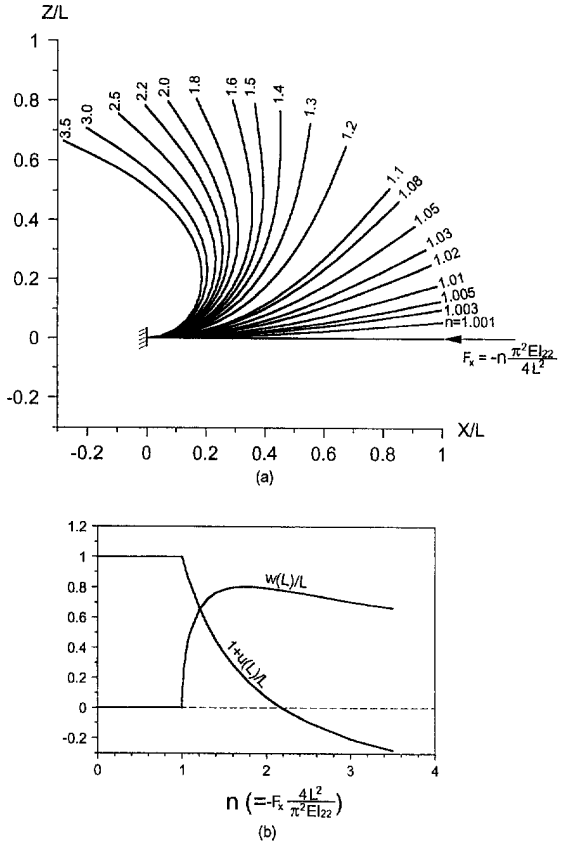

Fig. 3. The first-mode buckling of a cantilever: (a) the deformed configuration and (b) the force–end deflection curve.

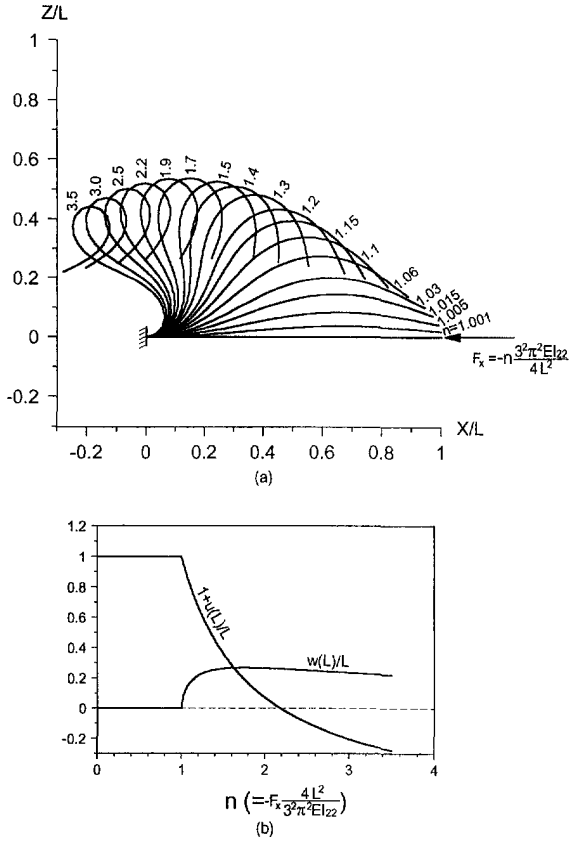

Fig. 4. The second-mode buckling of a cantilever: (a) the deformed configuration and (b) the force–end deflection curve.

$$F_{cr} = \frac{(2m-1)^2\pi^2 EI_{22}}{4L^2} \tag{28}$$

where m is the mode number of the buckled configuration.

The boundary conditions are

$$\begin{aligned} &\text{at } s = 0: \quad u = v = w = \phi = T_{13} = T_{12} = 0, \quad T_{11} = 1 \\ &\text{at } s = L: \quad F_y = F_z = M_1 = M_2 = M_3 = 0, \quad F_x = -n\frac{\pi^2 EI_{22}}{4L^2}. \end{aligned} \tag{29}$$

Figure 3 shows that when $n < 1.0$ there is no transverse deflection, which confirms the linear theory prediction. However, when $n > 1.0$, the transverse deflection is finite because deflections are limited by nonlinear structural terms, which is different from the linear theory prediction. Moreover, the force–end deflection curve shown in Fig. 3b is the same as that obtained by Sinclair (1979) for very thin beams. We point out here that 31 shooting points are used for Case II through Case VII.

III. *Second-mode buckling of cantilever* (*Fig.* 4)

For the buckling of cantilevers, most researchers studied the first-mode buckling. Because of initial imperfection and/or external constraints, other higher-mode buckling can also occur in real structures. For the second-mode buckling, the boundary conditions are

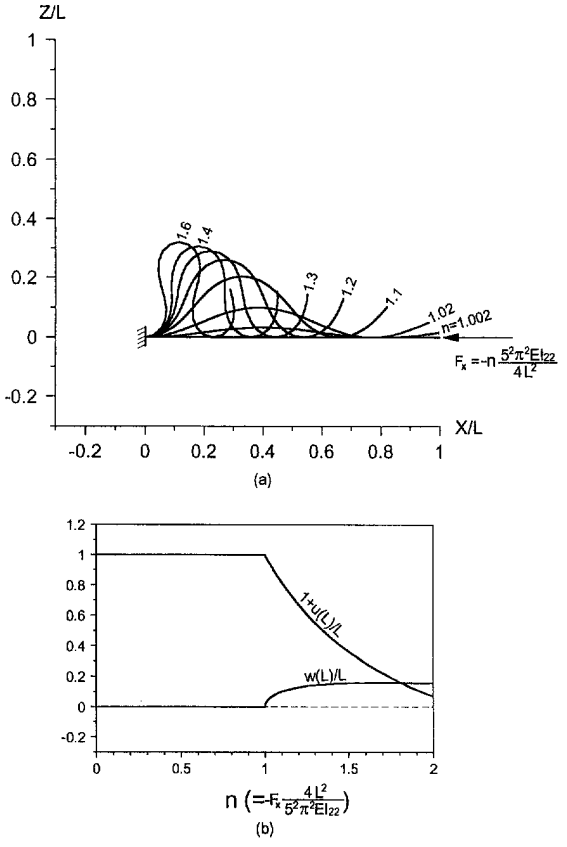

Fig. 5. The third-mode buckling of a cantilever: (a) the deformed configuration and (b) the force–end deflection curve.

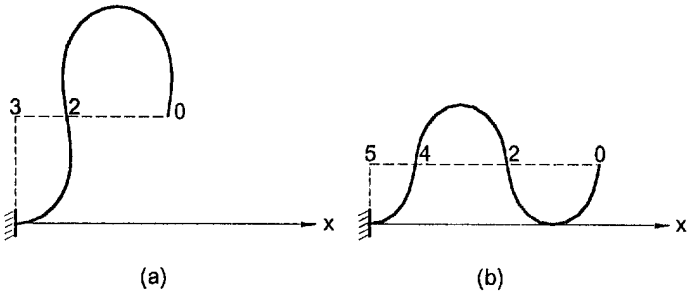

Fig. 6. The buckled configurations of a cantilever: (a) the second mode and (b) the third mode.

$$\text{at } s=0: \quad u=v=w=\phi=T_{13}=T_{12}=0, \quad T_{11}=1$$

$$\text{at } s=L: \quad F_y=F_z=M_1=M_2=M_3=0, \quad F_x=-n\frac{3^2\pi^2EI_{22}}{4L^2}. \tag{30}$$

Figure 4 shows that when $n<1.0$ there is no transverse deflection, which confirms the linear theory prediction.

IV. *Third-mode buckling of cantilever* (*Fig.* 5)

For the third-mode buckling, the boundary conditions are

$$\text{at } s=0: \quad u=v=w=\phi=T_{13}=T_{12}=0, \quad T_{11}=1$$

$$\text{at } s=L: \quad F_y=F_z=M_1=M_2=M_3=0, \quad F_x=-n\frac{5^2\pi^2EI_{22}}{4L^2}. \tag{31}$$

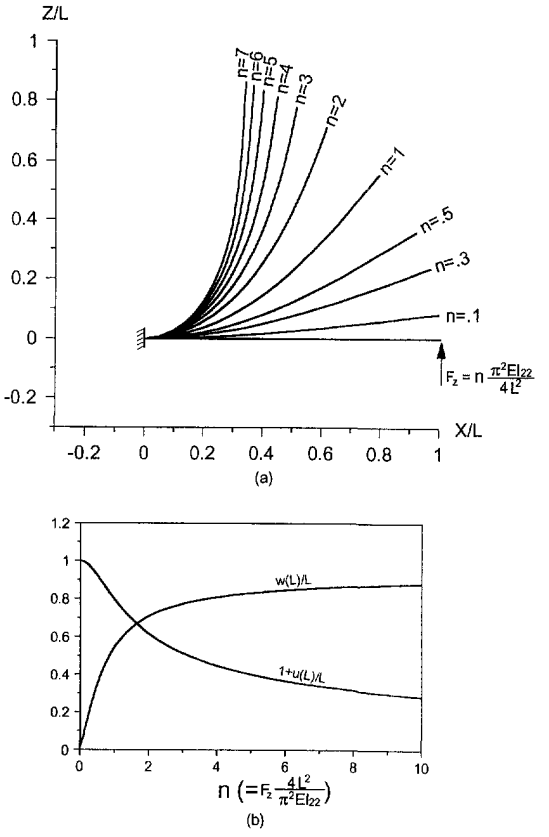

Fig. 7. The deformation of a cantilever subjected to a transverse end load F_3: (a) the deformed configuration and (b) the force–end deflection curve.

Figure 5 shows that when $n < 1.0$ there is no transverse deflection, which confirms the linear theory prediction.

The buckled configuration of the second mode (see Fig. 6a) shows the relation

$$\overline{02} = 2 \times \overline{23}, \tag{32}$$

where $\overline{02}$ is the distance shown in the figure from point 0 to 2. The buckled configuration of the third mode (see Fig. 6b) shows the relation

$$\overline{02} = \overline{24} = 2 \times \overline{45}. \tag{33}$$

However, the mode shapes are not cosine or sine functions.

We point out here that one axial load may correspond to several buckled configurations. For example, if $F_x = -30\pi^2 EI_{22}/4L^2$, the buckled shape can be that of the first mode, the second mode, or the third mode, or even a nonlinear combination of the first three modes. This reveals the characteristic of multiple solutions of a nonlinear system.

V. *Cantilever subjected to transverse end load (Fig. 7)*

The boundary conditions are

$$\text{at } s = 0: \quad u = v = w = \phi = T_{13} = T_{12} = 0, \quad T_{11} = 1$$

$$\text{at } s = L: \quad F_x = F_y = M_1 = M_2 = M_3 = 0, \quad F_z = n\frac{\pi^2 EI_{22}}{4L^2}. \tag{34}$$

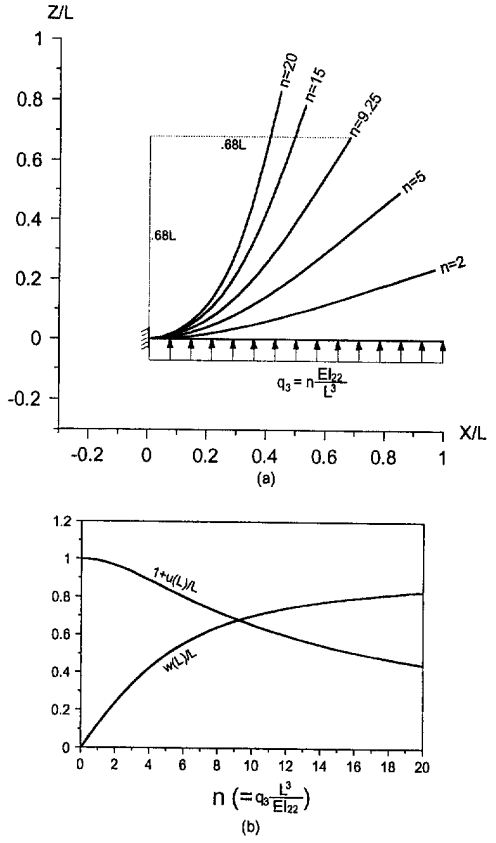

Fig. 8. The deformation of a cantilever subjected to a uniformly distributed transverse load q_3: (a) the deformed configuration and (b) the force–end deflection curve.

Figure 7a shows the exact deformed beam configurations and Fig. 7b shows the exact force–end deflection curve.

VI. *Cantilever subjected to uniformly distributed transverse load (Fig. 8)*

The distributed load is $q_3 = nEI_{22}/L^3$, which is always along the axis z even when the beam is bent. The boundary conditions are

$$\begin{aligned} &\text{at } s = 0: \quad u = v = w = \phi = T_{13} = T_{12} = 0, \quad T_{11} = 1 \\ &\text{at } s = L: \quad F_x = F_y = F_z = M_1 = M_2 = M_3 = 0. \end{aligned} \tag{35}$$

Figure 8a shows the exact deformed configurations and it also shows that, when $n = 9.25$, $L+u(L) = w(L) = 0.68L$. The force–end deflection curve shown in Fig. 8b is the same as that obtained by Sinclair (1979) and Holden (1972).

VII. *Fixed–free half circular ring subjected to tangential end load (Fig. 9)*

The planar deflection problem of a beam is the same as the cylindrical bending problem of a plate or a shell except that the flexural rigidity D is $D = EI_{22}$ for a beam and $D = Eh^3/12(1-\nu^2)$ for a plate or a shell. The material properties and beam geometry chosen for Cases VII and VIII are

$$\begin{aligned} &E = 1 \times 10^7 \text{ psi}, \quad \nu = 0.3 \\ &b = \tfrac{1}{4}\text{ in}, \quad h = \tfrac{1}{12}\text{ in}, \quad R = 5\text{ in}, \end{aligned} \tag{36}$$

which is the material used by Goto *et al.* (1992). Here R is the radius. The corresponding initial curvatures can be obtained as

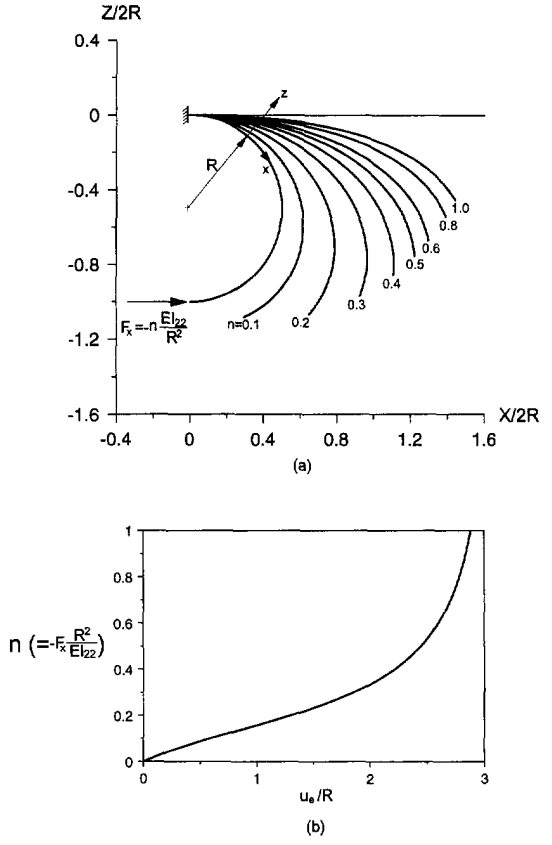

Fig. 9. The deformation of a fixed-free half circular ring subjected to a tangential force at the free end: (a) the deformed configuration and (b) the end deflection–force curve.

$$k_1 = k_3 = 0, \quad k_2 = \frac{1}{R}. \tag{37}$$

The boundary conditions are

$$\begin{aligned} &\text{at } s = 0: \quad u = v = w = \phi = T_{13} = T_{12} = 0, \quad T_{11} = 1 \\ &\text{at } s = R\pi: \quad F_y = F_z = M_1 = M_2 = M_3 = 0, \quad F_x = -n\frac{EI_{22}}{R^2}. \end{aligned} \tag{38}$$

Figure 9a shows the exact deformed configurations. The exact end deflection–force curve shown in Fig. 9b shows highly nonlinear phenomenon, where $u_e \equiv u|_{s=R\pi}$.

VIII. *Circular ring subjected to twisting* (*Fig.* 10)

We consider the deformation of a circular ring when it is twisted through an angle θ at one end of a diameter and an angle $-\theta$ at the other end, as shown in Fig. 10. The material properties and beam geometry are those shown in eqn (36). We note that one only needs to analyze one half of the ring and the deformations of the other half can be obtained by using the symmetry of the structural geometry and the skew-symmetry of the loading conditions as

$$u(\alpha) = -u(2\pi-\alpha), \quad v(\alpha) = -v(2\pi-\alpha), \quad w(\alpha) = w(2\pi-\alpha), \quad \phi(\alpha) = -\phi(2\pi-\alpha). \tag{39}$$

It follows from Fig. 10 that the boundary conditions are

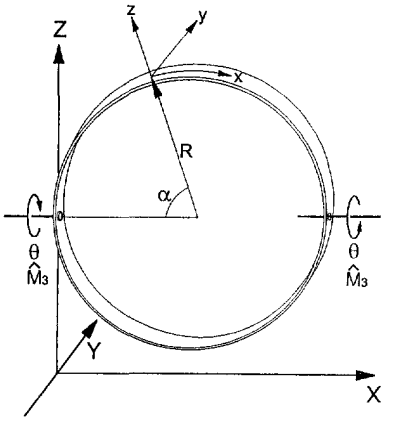

Fig. 10. A circular ring is twisted through an angle θ at both ends of a diameter, where the left end is immovable.

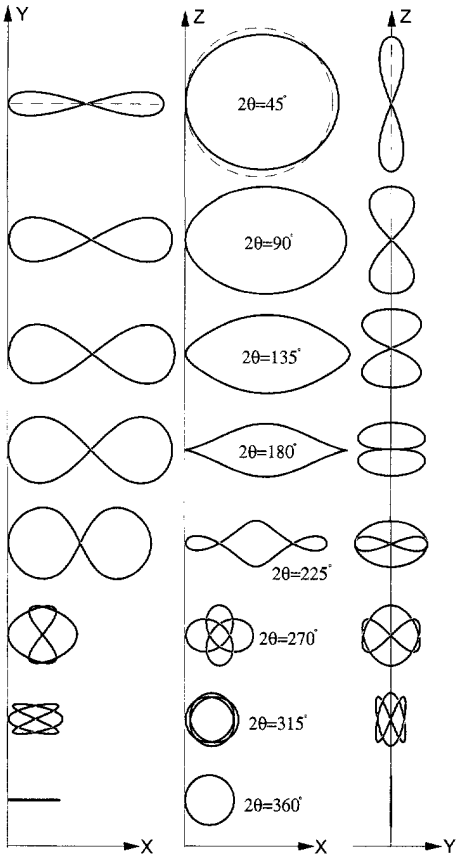

Fig. 11. The top, front and side views of a circular ring subjected to different magnitudes of twisting.

$$\text{at } s = 0: \quad u = v = w = \phi = T_{13} = 0, \quad T_{12} = \sin\theta, \quad T_{11} = \cos\theta$$
$$\text{at } s = R\pi: \quad u = v = F_z = \phi = T_{13} = 0, \quad T_{12} = \sin\theta. \tag{40}$$

Figure 11 shows the top view (i.e. projection onto the X–Y plane), front view (i.e. projection onto the X–Z plane) and side view (i.e. projection onto the Y–Z plane) for different magnitudes of twisting. We note that the ring is transformed into a small ring with a diameter of one-third of its original size when the ring is twisted by $2\theta = 360°$. Because very large bending rotations are involved, we use 81 shooting points for this problem.

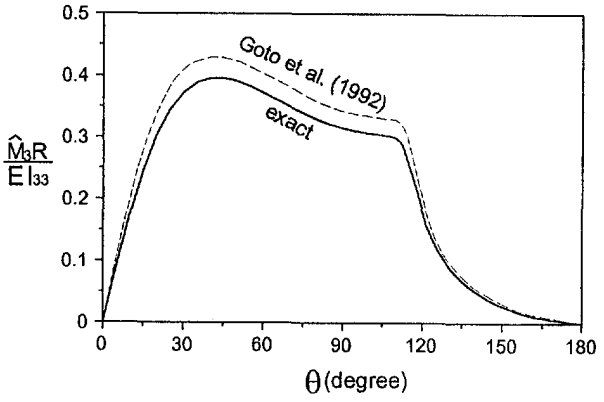

Fig. 12. The required end twisting moment $\hat{M}_3$ for different magnitudes of twisting.

Figure 12 shows the required end twisting moment $\hat{M}_3$ for different twisting angle θ. Although Goto *et al.* (1992) used 200 finite beam elements in modeling the half ring, there is still about 7.8% difference in the predicted maximum twisting moment. The difference may be due to the fact that they neglected the influence of initial curvatures [although initial curvatures were considered in their previous work (Goto *et al.*, 1985)] and/or because they used truncated Taylor expansions in their solution method. It is interesting that the deformed small ring can stay without any external force because $\hat{M}_3 = 0$ when $2\theta = 360°$.

Since $b \gg h$ and I_{33} is large, one may think that shear deformation might contribute very much to the transverse deformation v. As a matter of fact, v is mainly induced by the interaction of the transverse deflection w and the torsional deformation.

Figure 13a shows the distribution of ϕ and Fig. 13b shows its derivative. Figures 13b and c show that $\rho_1 \neq \phi'$ because ρ_1 accounts for relative twisting only but ϕ accounts for relative twisting and bending-induced rotations [see eqn (18j)]. In other words, ϕ does not really represent the twisting angle.

4. DISCUSSION

Although deformations of the reference line and large rotations of the observed cross section are exactly modeled in the presented nonlinear beam theory, some effects are not considered in the strain–displacement relation [eqn (15)] and the structural stiffness matrix in eqn (16). They are out-of-plane warpings due to transverse shears and torsions, in-plane warpings due to Poisson's effect and distributed external loadings, the restraint warping effect, the trapezoidal-edge effect and the induced extension–bending coupling due to initial bending curvatures and the extension–twisting coupling due to initial twisting. For composite and built-up beams, because of anisotropy and heterogeneity of materials, these effects can be significant and they can be coupled due to elastic couplings.

In-plane and out-of-plane warpings represent extra degrees of freedom for cross-section deformations and hence affect the structural stiffness values and extension–twisting and extension–bending couplings result in coupling stiffnesses in the structural stiffness matrix. The induced extension–bending coupling due to initial bending curvatures and the extension–twisting coupling due to initial twisting are significant for thick beams.

Warpings result in a three-dimensional stress state. To solve such a three-dimensional elasticity problem, a three-dimensional finite-element analysis may be the only way, which is too expensive in order to achieve certain accuracy. Starting from three-dimensional elasticity and using a perturbation analysis with slenderness ratio as the ordering parameter, Parker (1979a,b) showed that a combination of St Venant's warping solutions, which are derived from small displacement linear elasticity and a one-dimensional nonlinear beam model including large rotations is natural and can account for three-dimensional stress effects. More specifically, Berdichevskii (1981) stated that the geometrically nonlinear

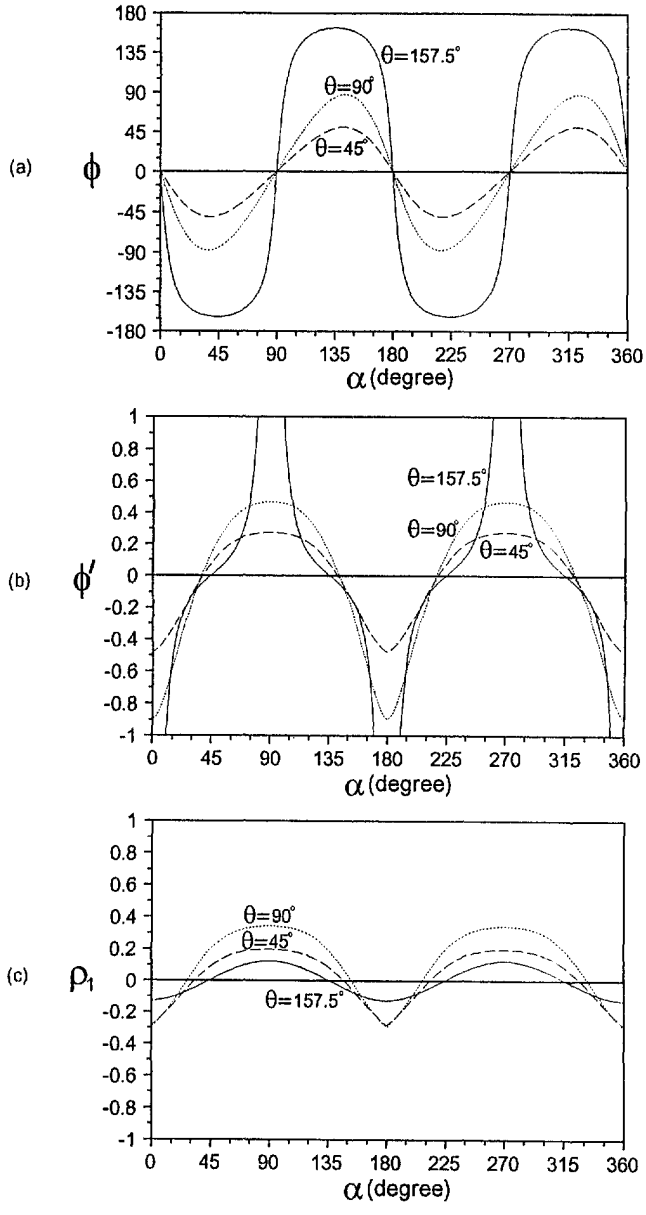

Fig. 13. The distributions of ϕ, ϕ', and ρ_1 when $\theta = 45°$, $\theta = 90°$, and $\theta = 157.5°$: (a) the α–ϕ curve, (b) the α–ϕ' curve and (c) the α–ρ_1 curve.

problem of the three-dimensional beam elasticity can be decoupled into a nonlinear one-dimensional problem and a linear two-dimensional section problem. In other words, a one-dimensional nonlinear beam model with structural stiffnesses and warping functions determined from a linear, static, two-dimensional sectional analysis is a general and practical approach in solving nonlinear anisotropic beam problems (Parker, 1979a,b; Berdichevskii, 1981; Borri and Merlini, 1986; Hodges, 1990).

Giavotto *et al.* (1983) presented a two-dimensional, static, sectional, finite-element analysis of St Venant's warping functions and boundary-layer warping solutions for straight beams, which formulation is linear and all variables are defined with respect to the undeformed coordinate system. Borri and Merlini (1986) extended the theory of Giavotto *et al.* (1983) to include geometric nonlinearities by using Green–Lagrange strains. Atilgan and Hodges (1991) presented a systematic, nonlinear formulation of the sectional analysis of straight beams, where geometric nonlinearities are accounted by using Green–Lagrange strains. Pai and Nayfeh (1994b) presented a formulation of using Jaumann stresses and

strains and the results of two-dimensional sectional analysis in the modeling of naturally curved and twisted composite rotor blades to account for warpings and three-dimensional stress effects.

Since only very thin and flexible isotropic beams with closed cross sections are considered here, all the effects due to warpings and three-dimensional stresses are neglected except that the torsional rigidity is modified to accounted for the torsional warping effect.

To account for transverse shear deformations, two more differential equations are needed [see eqns (18a–f) and eqns (60)–(65) of Pai and Nayfeh (1994b)]. To account for elastic couplings among bending, torsion and extension of composite beams, the stiffness matrix in eqn (16) needs to be replaced with a full matrix [see eqns (51a and c) of Pai and Nayfeh (1994b)].

5. CONCLUDING REMARKS

The numerical results show that the curved beam model does fully account for large rotations and displacements and effects due to initial curvatures and extensionality. Moreover, the use of the multiple shooting method in solving the highly nonlinear two-point boundary-value problem of flexible beams is efficient and promising. The obtained eight numerical solutions of flexible beam deformations are useful for checking the performance of nonlinear finite-element codes in analyzing large structural deformations.

Acknowledgement—This work was supported by the Air Force Office of Scientific Research and the Vehicle Subsystems Division of Wright Laboratory under grant no. F33600-93-R-0203. The first author is also supported by the NASA CORE Program (grant no. NAGW-2924).

REFERENCES

Alkire, K. (1984). An analysis of rotor blade twist variables associated with different Euler sequences and pretwist treatments. NASA TM 84394.

Atilgan, A. R. and Hodges, D. H. (1991). Unified nonlinear analysis for nonhomogeneous anisotropic beams with closed cross sections. *AIAA J.* **29,** 1990–1999.

Bathe, K. J. (1982). *Finite Elements Procedures in Engineering Analysis.* Prentice-Hall, Englewood Cliffs, NJ.

Bauchau, O. A. and Hong, C. H. (1987). Large displacement analysis of naturally curved and twisted composite beams. *AIAA J.* **25,** 1469–1475.

Berdichevskii, V. L. (1981). On the energy of an elastic rod. *J. Appl. Math. Mech.* (*PMM U.S.S.R.*) **45,** 518–529.

Berdichevskii, V. L. and Staroselsky, L. A. (1979). On the theory of naturally twisted curvilinear rods. *MTT* **14,** 87–95.

Borri, M. and Merlini, T. (1986). A large displacement formulation for anisotropic beam analysis. *Meccanica* **21,** 30–37.

Cesnik, C. E. S. and Hodges, D. H. (1993). Variational-asymptotical analysis of initially curved and twisted composite beams. *Appl. Mech. Rev.* **46,** S211–S220.

Giavotto, V., Borri, M., Mantegazza, P., Ghiringhelli, G., Carmaschi, V., Maffioli, G. C. and Mussi, F. (1983). Anisotropic beam theory and applications. *Comput. Struct.* **16,** 403–413.

Goto, Y., Matsuura, S., Hasegawa, A., and Nishino, F. (1985). A new formulation of finite displacement theory of curved and twisted rods. In: *Proc. of JSCE Structural Engineering/Earthquake Engineering*, Vol. 2, pp. 119–129.

Goto, Y., Watanabe, Y., Kasugai, T. and Obata, M. (1992). Elastic buckling phenomenon applicable to deployable rings. *Int. J. Solids Structures* **29,** 893–909.

Henderson, B. W. (1990). Boeing Condor raises UAV performance levels. *Aviation Week Space Technol.* **132,** 36–38.

Hodges, D. H. (1990). A mixed variational formulation based on exact intrinsic equations for dynamics of moving beams. *Int. J. Solids Structures* **26,** 1253–1273.

Holden, J. T. (1972). On the finite deflections of thin beams. *Int. J. Solids Structures* **8,** 1051–1055.

Horrigmoe, G. and Bergan, P. G. (1978). Instability analysis of free form shells by flat finite elements. *Comput. Meth. Appl. Mech. Engng* **16,** 11–35.

Malvern, L. E. (1969). *Introduction to the Mechanics of a Continuous Medium.* Prentice-Hall, Englewood Cliffs, NJ.

Minguet, P. and Dugundji, J. (1990). Experiments and analysis for composite blades under large deflections, Part I. static behavior. *AIAA J.* **28,** 1573–1579.

Nygard, M. K. and Bergan, P. G. (1989). Advances in treating large rotations for nonlinear problems. In: *State-Of-The-Art Surveys on Computational Mechanics* (Edited by A. K. Noor and J. T. Oden), pp. 305–333. American Society of Mechanical Engineers.

Oden, J. T. (1972). *Finite Elements of Nonlinear Continua.* McGraw-Hill, New York.

Pai, P. F. and Nayfeh, A. H. (1991). A nonlinear composite plate theory. *Nonlin. Dyn.* **2,** 445–477.

Pai, P. F. and Nayfeh, A. H. (1994a). A new method for the modeling of geometric nonlinearities in structures. *Comput. Struct.* **53,** 877–895.

Pai, P. F. and Nayfeh, A. H. (1994b). A fully nonlinear theory of curved and twisted composite rotor blades accounting for warpings and three-dimensional stress effects. *Int. J. Solids Structures* **31,** 1309–1340.

Pai, P. F. and Palazotto, A. N. (1995). Polar decomposition theory in nonlinear analyses of solids and structures. *J. Engng Mech.* **121,** 568–581.

Palazotto, A. N. and Dennis, S. T. (1992). *Nonlinear Analysis of Shell Structures.* American Institute of Aeronautics and Astronautics, Washington, DC.

Parker, D. F. (1979a). An asymptotic analysis of large deflections and rotations of elastic rods. *Int. J. Solids Structures* **15,** 361–377.

Parker, D. F. (1979b). The role of Saint Venant's solutions in rod and beam theories. *J. Appl. Mech.* **46,** 861–866.

Pestel, E. C. and Leckie, F. A. (1963). *Matrix Methods in Elastomechanics.* McGraw-Hill, Maidenhead.

Reissner, E. (1973). On one-dimensional large-displacement finite-strain beam theory. *Stud. Appl. Math.* **52,** 87–95.

Riks, E. (1979). An incremental approach to the solution of snapping and buckling problems. *Int. J. Solids Structures* **15,** 524–551.

Sewell, G. (1982). IMSL software for differential equations in one space variable. IMSL Technical Report 8202, IMSL, Houston.

Sinclair, G. B. (1979). The nonlinear bending of a cantilever beam with shear and longitudinal deformations. *Int. J. Nonlin. Mech.* **14,** 111–122.

Stemple, A. D. and Lee, S. W. (1988). Finite-element model for composite beams with arbitrary cross-sectional warping. *AIAA J.* **26,** 1512–1520.

Stone, R. G. (1965). RAE-1500 ft. antenna satellite. *Astronaut. Aeronaut.* **3,** 46–49.

Timoshenko, S. P. and Gere, J. M. (1961). *Theory of Elastic Stability.* McGraw-Hill, New York.

Timoshenko, S. P. and Goodier, J. N. (1970). *Theory of Elasticity,* 3rd Edn. McGraw-Hill, New York.

Wang, C. Y. (1991). Postbuckling of an externally pressurized ring with a hinge. *Int. J. Solids Structures* **27,** 1287–1293.

Wriggers, P. and Simo, J. C. (1990). A general procedure for the direct computation of turning and bifurcation points. *Int. J. Numer. Meth. Engng* **30,** 155–176.